Computation of Induced Fields Into the Human Body by Dual Finite Element Formulations

Riccardo Scorretti[1], Ruth V. Sabariego[2], Laurent Morel[1], Christophe Geuzaine[2], Noel Burais[1], and Laurent Nicolas[1]

[1]Laboratoire Ampère-UMR 5005 CNRS, University of Lyon, 69622 Villeurbanne, France
[2]Dept. Electrical Engineering and Computer Science (ACE) University of Liège, Sart Tilman B28, B-4000 Liège, Belgium

In this work we present two dual finite element formulations to compute extremely low frequency (ELF) induced fields into the human body. This allows to estimate the numerical error, as well as rigorously bound the (global) co-energy. This method is herein applied to the classical case of the exposure to a homogeneous magnetic field, and to the field generated by an infinite wire.

Index Terms—**Dosimetry, extremely low frequencies, finite element methods, phantoms.**

I. Introduction

NUMERICAL dosimetry of extremely low frequency (ELF) fields induced in the human body is important in order to better tune and/or understand the effects of recent medical devices based on electrical energy [1], and for limiting human exposure to electromagnetic fields [2]. Due to the difficulty of obtaining high quality meshes from segmented images, most computations are performed by means of finite difference (FD) methods [3], [4] as they are straightforwardly applied to "hexahedral" meshes. Despite the effort of the scientific community, a convincing validation of numerical simulations is still missing: nowadays, the only possible assessment of the reliability of dosimetric simulations is to perform inter-laboratory comparisons [5], [6]. Some experimental measurements of the induced electric field have been performed in the past by Miller [7] by using microelectrodes. However this technique is extremely invasive, what greatly limits the number of measurement points. Moreover, the perturbation on the electric field due to the electrode itself is an issue. More recently, promising results in both radio and low frequency [8], [9] have been obtained with MRI based techniques. More fundamental problems are the anisotropy of some tissues [10] (in particular the skeletal muscles), the variability [11], [12], and the lack of knowledge about the dielectric properties of tissues. This last issue seems particularly problematic at ELF frequencies: in a recent work [13] Gabriel *et al.* have performed new measurements for a limited number of organs, and found large differences with respect to previously published data [14]. Even when only the numerical aspects are addressed, numerical errors may be large, therefore it is important to quantify them.

II. Formulations for Numerical Dosimetry

In the quasi-static approximation, Maxwell's equations for a magnetodynamic problem are:

$$\operatorname{curl}\mathbf{e} = -\partial_t\mathbf{b},\ \operatorname{curl}\mathbf{h} = \mathbf{j},\quad \operatorname{div}\mathbf{b} = 0, \qquad \text{(1a,b,c)}$$

$$\mathbf{j} = \sigma\mathbf{e},\quad \mathbf{b} = \mu\mathbf{h} \qquad \text{(1d,e)}$$

Manuscript received July 07, 2011; revised September 30, 2011; accepted October 21, 2011. Date of current version January 25, 2012. Corresponding author: R. Scorretti (e-mail: Riccardo.Scorretti@univ-lyon1.fr

with $\mathbf{e}$ the electric field, $\mathbf{h}$ the magnetic field, $\mathbf{j}$ the electric current density, $\mathbf{b}$ the magnetic flux density, σ the electrical conductivity and μ the magnetic permeability. Due to the large average conductivity of tissues, the conduction currents are dominant with regard to the displacement currents ($\sigma \simeq 0.4\,\mathrm{S/m} \gg \omega\epsilon$), and the latter can be neglected. Besides, at ELF frequencies with such a conductivity, the skin depth is of hundreds of meters, which allows to neglect the effect of the reaction field as well:

$$\mathbf{b} = \operatorname{curl}\mathbf{a} \simeq \mathbf{b_s} = \operatorname{curl}\mathbf{a_s} \qquad \text{(1f)}$$

$$\mathbf{e} = -\partial_t\mathbf{a} - \operatorname{grad}\phi \simeq -\partial_t\mathbf{a}_s - \operatorname{grad}\phi \qquad \text{(1g)}$$

where $\mathbf{b_s}$ is the imposed flux density to which the body is exposed. The computational domain can thus be restricted to the human body [15] with an imposed boundary condition at its surface given by: $\mathbf{n}\cdot\mathbf{j}|\partial\Omega = 0$. At the continuous level, these fields (together with associated potentials—see below) can be organized in the following Tonti's diagram [16]:

$$\begin{array}{ccccccc} \phi & \xrightarrow{\text{grad}} & \mathbf{e},\mathbf{a} & \xrightarrow{\text{curl}} & \mathbf{b} & \xrightarrow{\text{div}} & 0 \\ & & \sigma\updownarrow & & \mu\updownarrow & & \\ 0 & \xleftarrow{\text{div}} & \mathbf{j} & \xleftarrow{\text{curl}} & \mathbf{h},\mathbf{t} & & \end{array} \qquad (2)$$

At the discrete level this structure is approximated by appropriate mixed finite elements (FE). Two dual formulations are obtained by strongly imposing the constitutive laws (1d,e) and either Faraday's law (1a) or Ampère's law (1b), associated, respectively, to the upper and lower level of (2), whereas the equation linked to the other level is weakly imposed [16].

A. The *e*—conform ϕ—$\mathbf{a}$ formulation

Let $\mathbf{a}$ be a *known* magnetic vector potential such that: $\operatorname{curl}\mathbf{a} = \mathbf{b}$. By enforcing in a strong sense the upper level of (2), i.e., Faraday's law (1a) one obtains that: $\mathbf{e} = -\partial_t\mathbf{a} - \operatorname{grad}\phi$, where ϕ is an unknown electric scalar potential. The weak form of Ampère's law (1b) reads [15]: Find $\phi\epsilon\mathrm{H}(\operatorname{grad},\Omega)$ such that

$$(\sigma(\partial_t\mathbf{a} + \operatorname{grad}\phi), \operatorname{grad}\phi') = 0 \quad \forall\phi'\epsilon\mathrm{H}(\operatorname{grad},\Omega) \qquad (3)$$

where $(\cdot,\cdot)$ denotes a volume integral in Ω of the product of vector fields, and: $\mathbf{H}(\operatorname{grad},\Omega) = \{\phi\epsilon\mathrm{L}^2(\Omega) : \int_\Omega \|\operatorname{grad}\phi(\mathbf{x})\|^2\mathbf{dx} < \infty\}$.

B. The *j*—Conform $\mathbf{t}-\mathbf{b}$ Formulation

Analogously, we can strongly enforce the lower level of (2), i.e. the divergence of Ampère's law (1b), $\operatorname{div}\mathbf{j} = 0$. Let $\mathbf{t}$ be

an unknown electric vector potential such that: $\text{curl}\ \mathbf{t} = \mathbf{j}$. The weak form of Faraday's law (1a) is given by [17]: Find $\mathbf{t}\epsilon\mathbf{H}_0(\text{curl},\Omega)$ such that

$$\left(\frac{1}{\sigma}\text{curl}\ \mathbf{t},\ \text{curl}\ \mathbf{t}'\right) + (\partial_t \mathbf{b},\ \mathbf{t}') = 0 \quad \forall \mathbf{t}'\epsilon\mathbf{H}_0(\text{curl},\Omega) \quad (4)$$

where: $\mathbf{H}_0(\text{curl},\Omega) = \{\mathbf{f}\epsilon\mathbf{L}^2(\Omega) : \int_\Omega ||\text{curl}\ \mathbf{f}(\mathbf{x})||^2\ \mathbf{dx} < \infty, \mathbf{n}\times\mathbf{f}|_{\partial\Omega} = 0\}$. However, this formulation gives rise to a badly conditioned linear system when the imposed flux density $\mathbf{b}$ is not exactly solenoidal. This drawback can be overcome [18] by projecting $\mathbf{b}$ on the kernel of the div operator $\mathbf{H}(\text{div}\ 0,\Omega)$. That is, a vector potential $\mathbf{a}$ such that $\mathbf{b} = \text{curl}\ \mathbf{a}$ is computed [19] and (4) becomes: Find $\mathbf{t}\epsilon\mathbf{H}_0(\text{curl},\Omega)$ such that

$$\left(\frac{1}{\sigma}\text{curl}\ \mathbf{t},\ \text{curl}\ \mathbf{t}'\right) + (\partial_t \mathbf{a},\ \text{curl}\ \mathbf{t}') = 0 \quad \forall \mathbf{t}'\epsilon\mathbf{H}_0(\text{curl},\Omega), \quad (5)$$

This ungauged formulation gives rise to a singular linear system, which is effectively solved by using GMRES preconditioned by Jacobi.

III. Error Estimate and Co-Energy Bound

Considering the dual electromagnetic formulations together allows, on the one hand, to calculate a more precise solution as the average of the two dual solutions:

$$\mathbf{e} = \frac{1}{2}\left(\mathbf{e}_1 + \frac{1}{\sigma}\mathbf{j}_2\right) = \frac{1}{2}\left(-\partial_t\mathbf{a} - \text{grad}\phi + \frac{1}{\sigma}\text{curl}\ \mathbf{t}\right) \quad (6)$$

where $\mathbf{e}_1$ and $\mathbf{j}_2$ are computed respectively with the $\phi - \mathbf{a}$ and $\mathbf{t} - \mathbf{b}$ conform formulation. On the other hand, the relative numerical error can be estimated as [6]

$$\Delta\% = 2\frac{||\mathbf{e}_1 - \frac{\sigma}{1}\mathbf{j}_2||}{||\mathbf{e}_1 + \frac{1}{\sigma}\mathbf{j}_2||}\times 100\%. \quad (7)$$

A rigorous bound can be found for the (global) electric coenergy $\mathcal{E}^C$, which is defined as

$$\mathcal{E}^C = \int_\Omega \int_0^{\mathbf{e}} \mathbf{j}\mathrm{d}\mathbf{e}. \quad (8)$$

For the sake of simplicity, assume that all materials are linear. At the continuous level, $\mathcal{E}^C$ may be expressed as:

$$\mathcal{E}^C = \frac{1}{2}\int_\Omega \sigma\mathbf{e}\cdot\mathbf{e}\mathrm{d}\Omega = \int_\Omega \mathbf{j}\cdot\mathbf{e}\mathrm{d}\Omega - \frac{1}{2}\int_\Omega \mathbf{j}\cdot\frac{1}{\sigma}\mathbf{j}\mathrm{d}\Omega. \quad (9)$$

At the discrete level, the continuous fields are replaced by $\mathbf{e}_1$ and $\mathbf{j}_2$, so that we obtain two discrete coenergies

$$\mathcal{E}1^C = \frac{1}{2}(\sigma\mathbf{e}_1,\mathbf{e}_1) \quad (10)$$

$$\mathcal{E}_2^C = (\mathbf{e}_1,\mathbf{j}_2) - \frac{1}{2}\left(\frac{1}{\sigma}\mathbf{j}_2,\ \mathbf{j}_2\right). \quad (11)$$

The local Ohm's law is not exactly verified (that is $\mathbf{j}_2 \neq \sigma\mathbf{e}_1$), thus (9) does not hold anymore for the discrete coenergies. However, at the discrete level, this can be exploited as the two coenergies represent a lower and an upper bound for the continuous (exact) coenergy:

$$\mathcal{E}_1^C \geq \mathcal{E}^C \geq \mathcal{E}_2^C. \quad (12)$$

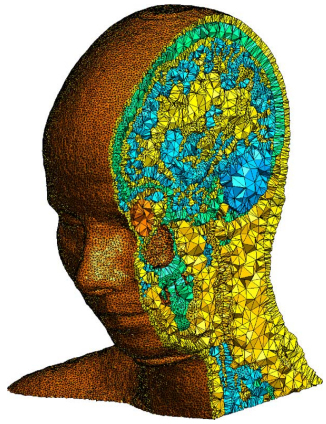

Fig. 1. Mesh of the phantom "Ella", each color corresponds to a tissue.

The derivation of (12) is reported in Appendix A. Herein, the energy bounds, established for other static formulations in [16], [20]–[22], are adapted to the proposed electrodynamic formulations $\phi - \mathbf{a}$ and $\mathbf{t} - \mathbf{b}$, specially modified to handle the complex biomedical context of the application.

IV. The Computational Phantoms

Several computational phantoms have been used in this work: i) a homogeneous ellipsoid, ii) the "Zol" phantom, based on the Visible Human Project (VHP), iii) the "Ella" phantom, based on the Virtual Family [23]. The phantom "Zol" is a Caucasian male; it has been meshed with the software AMIRA, starting from the segmented images formerly available from the US Brooks Air Force Base [5]. It comprises $84\cdot 10^3$ nodes, and 17 different tissues are identified. The phantom "Ella" represents a Caucasian woman (Fig. 1). The mesh was generated from the 1 mm voxel model by means of the free toolbox ISO2MESH [24]. The minimal targeted length of the edges of tetrahedra is 2 mm for the whole body mesh, and 1.5 mm for two partial meshes, limited to the head and to the trunk. In the original phantom, 77 different tissues are identified. In order to relax the constraints on internal surfaces, some tissues with similar conductivities have been merged together during the meshing step. In particular, we distinguish the "cartilage-like", the "bone-like", the "muscle-like" and the "fat-like" tissues, the last type with very low conductivity at 50 Hz. The eyes constitute also a unique region, as meshing extremely thin regions like the corneas was not feasible. The final whole body mesh comprises more than 1 million nodes with 45 different tissues. For all simulations, we use the conductivity values reported in [14].

V. Numerical Results

A. Exposure to a Uniform Field

We simulate the exposure of a homogeneous ellipsoid to a vertical homogeneous 500 μT flux density at 50 Hz. The bound (12) has been checked with progressively refined meshes (Table I), clearly confirming the expected results. In order to test the error estimate with a more realistic phantom, we simulated the exposure to a uniform magnetic field with the Zol phantom. The computation with the dual formulations has been performed by using first-order and second-order hierarchical shape functions. We evaluated the electric field and the error estimate $\Delta\%$ at the barycenter of each element. We observe

TABLE I
DISCRETE COENERGIES FOR AN ELLIPSOID (μJ)

No of nodes	$\mathcal{E}_1^C$	$\mathcal{E}_2^C$	$\mathcal{E}_1^C - \mathcal{E}_2^C$
250	20.1750	18.4617	1.7133
$3{\cdot}10^3$	20.1197	19.7165	0.4032
$10{\cdot}10^3$	20.1047	19.9801	0.1246
$75{\cdot}10^3$	20.0937	20.0771	0.0166

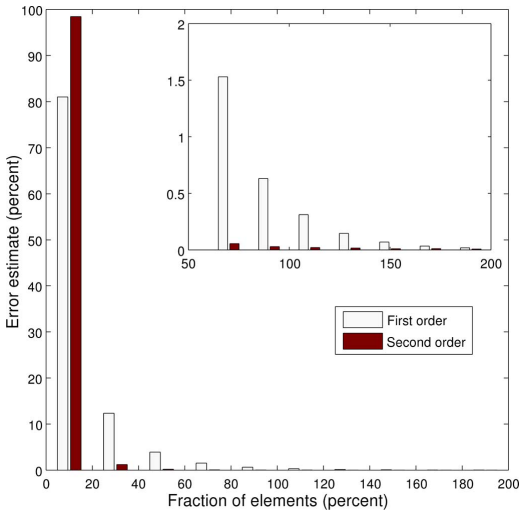

Fig. 2. Hystogram of the error estimates (inset: zoom of the queue).

that the $\Delta\%$ obtained with high order functions is globally much smaller than with first order functions. The histograms of $\Delta\%$ first and second order (empty and filled bars) are depicted in Fig. 2. We observe that the $\Delta\%$ obtained with high order functions is globally much smaller than with first order functions, e.g. $\Delta\% < 10\%$ for the 81% and the 98% of the elements with first and second order functions, respectively. Moreover, 89% of the values computed with high order functions are included in the error bars computed with first order functions, i.e. $\|\mathbf{e}^{\mathrm{H}} - \mathbf{e}\| < \|\mathbf{e}_1 - \mathbf{j}_2/\sigma\|$, where $\mathbf{e}^{\mathrm{H}}$ is computed with high order functions.

B. Exposure to The Field Generated by a Wire

We simulate with the Ella phantom the exposure to the field due to an infinite cable (current $I = 1000$ A at 50, Hz) placed at a few centimeters from the left side of the head (Fig. 3). We observe that most of the induced current flows through the cerebrospinal fluid, as its conductivity ($\sigma = 2$ S/m) is much higher than the conductivity of nervous tissues ($\sigma < 0.1$ S/m). For each tissue, we compute the maximum value of $\|\mathbf{e}\|$, the 99% percentile (i.e. the maximum value after removal of the 1% highest values [2], [25]), and the corrected maximum value $\max^*\|\mathbf{e}\|$ obtained after removal of the 1% of the elements with the highest error estimate $\Delta\%$. In general the elements with the highest error do not match the ones with the highest values of the field (Table II): if it were the case, the 99% percentile and $\max^*\|\mathbf{e}\|$ should be the same. This could be important as, according to the last ICNIRP guidelines [2], the limit of exposure is based on the 99% percentile of the electric field, averaged on a small cube (side 2 mm). From the point of view of numerical dosimetry, it would be interesting to obtain strong bounds for such averaged fields [22].

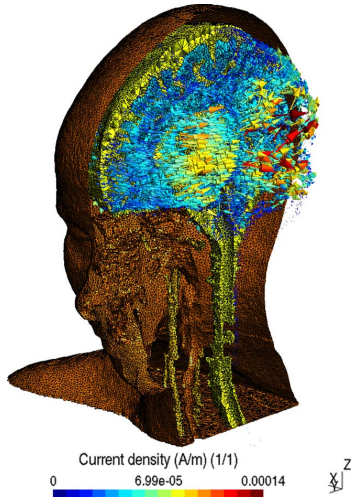

Fig. 3. Current density induced by a cable.

TABLE II
MAX, 99% PERCENTILE AND $\max^*\|\mathbf{e}\|$ FOR SOME TISSUES (mV/m)

Tissue	max $\|$ e $\|$	99% percentile	max* $\|$ e $\|$
Grey matter	274	62	238
White matter	101	49	101
Cerebellum	146	37	72
Nerve	50	36	49
Eyes	17	8.3	17
Bones	260	86	260
Muscle	90	41	90
Fat	199	66	199

VI. CONCLUSION

We use two dual formulations for computing induced electromagnetic fields at power frequencies. This allows to obtain an effective estimate of the numerical error, at the expense of a higher computation time. Computations have been performed with numerical phantoms with high resolutions close to the state-of-the-art models—which is a novelty for a FE dosimetric simulation.

APPENDIX A
PROOF OF THE COENERGY BOUND

The continuous $\phi - \mathbf{a}$ formulation can be rewritten as a minimization problem:

$$\begin{aligned}\phi &= \underset{\phi' \in \mathrm{H(grad},\Omega)}{\arg\min}\ \mathcal{E}_1^C[\phi'] \\ &= \underset{\phi' \in \mathrm{H(grad},\Omega)}{\arg\min}\ \frac{1}{2}\left(\sigma(\partial_t \mathbf{a} + \mathrm{grad}\phi'), \partial_t \mathbf{a} + \mathrm{grad}\phi'\right) \quad (13)\end{aligned}$$

Let $\eta \neq 0\ \epsilon \mathrm{H(grad},\Omega)$ be an arbitrary scalar potential; assuming that ϕ is solution of (3) we obtain:

$$\begin{aligned}\mathcal{E}_1^C[\phi+\eta] &= \mathcal{E}_1^C[\phi] + \mathcal{E}_1^C[\eta] + (\sigma(\partial_t \mathbf{a} + \mathrm{grad}\phi), \mathrm{grad}\eta) \\ &= \mathcal{E}_1^C[\phi] + \mathcal{E}_1^C[\eta] \geq \mathcal{E}_1^C[\phi]\end{aligned}$$

When ϕ is the solution of the discretized formulation, (13) is minimized over a discrete subset of $\mathrm{H(grad},\Omega)$, thus: $\mathcal{E}_1^C = \mathcal{E}_1^C[\phi] \geq \mathcal{E}^C$.

Similarly, the continuous $\mathbf{t}-\mathbf{b}$ formulation can be rewritten as a maximization problem:

$$\begin{aligned}\mathbf{t} &= \underset{\mathbf{t}'\epsilon\mathbf{H}_0(\mathrm{curl},\Omega)}{\arg\max}\ \mathcal{E}_2^C[\mathbf{t}'] \\ &= \underset{\mathbf{t}'\epsilon\mathbf{H}_0(\mathrm{curl},\Omega)}{\arg\max}\ (\mathbf{e}_1,\mathrm{curl}\,\mathbf{t}') - \frac{1}{2}\left(\frac{1}{\sigma}\mathrm{curl}\,\mathbf{t}',\mathrm{curl}\,\mathbf{t}'\right) \quad (14)\end{aligned}$$

Note that $\mathcal{E}_2^C[\mathbf{t}']$ does not depend on ϕ:

$$\begin{aligned}(\mathbf{e}_1,\mathrm{curl}\,\mathbf{t}') &= (-\partial_t\mathbf{a}-\mathrm{grad}\phi,\mathrm{curl}\,\mathbf{t}') \\ &= -(\partial_t\mathbf{a},\mathrm{curl}\,\mathbf{t}')\end{aligned}$$

because the remaining term $(\mathrm{grad}\,\phi,\mathrm{curl}\,\mathbf{t}')$ vanishes by:

$$(\mathrm{grad}\phi,\mathrm{curl}\,\mathbf{t}') = -(\phi,\mathrm{div}\,\mathrm{curl}\,\mathbf{t}') + \langle\phi,\mathbf{n}\cdot\mathrm{curl}\,\mathbf{t}'\rangle = 0$$

where $\langle\cdot,\cdot\rangle$ denotes a surface integral on $\partial\Omega$, and $\mathbf{n}\times\mathbf{t}'|_{\partial\Omega} = 0 \ \Rightarrow \mathbf{n}\cdot\mathrm{curl}\,\mathbf{t}' = 0$.

Assuming that $\mathbf{t}$ is solution of (5) and taking an arbitrary vector potential $\mathbf{g}\epsilon\mathbf{H}_0(\mathrm{curl},\Omega)$ we obtain:

$$\begin{aligned}\mathcal{E}_2^C[\mathbf{t}+\mathbf{g}] &= \mathcal{E}_2^C[\mathbf{t}] - \frac{1}{2}\left(\frac{1}{\sigma}\mathbf{g},\mathbf{g}\right) \\ &\quad - \left[\left(\frac{1}{\sigma}\mathrm{curl}\,\mathbf{t},\mathrm{curl}\,\mathbf{g}\right) + (\partial_t\mathbf{a},\mathrm{curl}\,\mathbf{g})\right]. \\ &= \mathcal{E}_2^C[\mathbf{t}] - \frac{1}{2}\left(\frac{1}{\sigma}\mathbf{g},\mathbf{g}\right) \le \mathcal{E}_2^C[\mathbf{t}]\end{aligned}$$

However, when $\mathbf{t}$ is the solution of the discretized formulation, (14) can be maximized only over a discrete subset of $\mathbf{H}_0(\mathrm{curl},\Omega)$, thus we obtain: $\mathcal{E}^C \ge \mathcal{E}_2^C[\mathbf{t}] = \mathcal{E}_2^C$. Finally

$$\mathcal{E}_1^C = \mathcal{E}_1^C[\phi] \ge \mathcal{E}^C \ge \mathcal{E}_2^C[\mathbf{t}] = \mathcal{E}_2^C.$$

ACKNOWLEDGMENT

R. Scorretti thanks the ACE, University of Liège for the invitation which allowed this work, and P. Jeandel for her assistance with informatic problems. This work was supported in part by the Belgian BioElectroMagnetic Group (BBEMG) EMF programme.

REFERENCES

[1] A. Ivorra, B. Al-Sakere, B. Rubinsky, and L. M. Mir, "In vivo electrical conductivity measurements during and after tumor electroporation: Conductivity changes reflect the treatment outcome," *Phys. Med. Biol.*, vol. 54, no. 19, pp. 5949–5963, Oct. 2009.

[2] ICNIRP, "Guidelines for limiting exposure to time-varying electric and magnetic fields (1 Hz to 100 kHz)," *Health Phys.*, vol. 99, no. 6, pp. 818–836, 2010.

[3] P. J. Dimbylow, "Induced current densities from low-frequency magnetic fields in a 2 mm resolution, anatomically realistic model of the body," *Phys. Med. Biol.*, vol. 43, no. 2, pp. 221–230, Feb. 1998.

[4] P. Dimbylow, "Development of pregnant female, hybrid voxel-mathematical models and their application to the dosimetry of applied magnetic and electric fields at 50 Hz," *Phys. Med. Biol.*, vol. 51, no. 10, pp. 2383–2394, May 2006.

[5] K. Caputa, P. J. Dimbylow, T. W. Dawson, and M. A. Stuchly, "Modelling fields induced in humans by 50/60 Hz magnetic fields: Reliability of the results and effects of model variations," *Phys. Med. Biol.*, vol. 47, no. 8, pp. 1391–1398, Apr. 2002.

[6] M. A. Stuchly and O. P. Gandhi, "Inter-laboratory comparison of numerical dosimetry for human exposure to 60 Hz electric and magnetic fields," *Bioelectromagnetics*, vol. 21, no. 3, pp. 167–174, Apr. 2000.

[7] D. L. Miller and J. A. Creim, "Comparison of cardiac and 60 Hz magnetically induced electric fields measured in anesthetized rats," *Bioelectromagnetics*, vol. 18, no. 4, pp. 317–323, Jan. 1997.

[8] I. Sersa, K. Beravs, N. J. Dodd, S. Zhao, D. Miklavcic, and F. Demsar, "Electric current density imaging of mice tumors," *Mag. Res. Med.*, vol. 37, no. 3, pp. 404–409, Mar. 1997.

[9] H. J. Kim, Y. T. Kim, A. S. Minhas, W. C. Jeong, E. J. Woo, J. K. Seo, and O. J. Kwon, "In vivo high-resolution conductivity imaging of the human leg using MREIT: The first human experiment," *IEEE Trans. Med. Imag.*, vol. 28, no. 11, pp. 1681–1687, 2009.

[10] F. Sachse, M. Wolf, C. Werner, and K. Meyer-Waarden, "Extension of anatomical models of the human body: Three-dimensional interpolation of muscle fiber orientation based on restrictions," *J. Comp. Inf. Tech.*, vol. 6, no. 1, pp. 95–101, 1998.

[11] C. Gabriel, "Dielectric properties of biological tissue: Variation with age," *Bioelectromagnetics*, vol. Suppl 7, pp. S12–S18, Jan. 2005.

[12] S. Whalen, C. Lee, J. L. Williams, and W. E. Bolch, "Anthropometric approaches and their uncertainties to assigning computational phantoms to individual patients in pediatric dosimetry studies," *Phys. Med. Biol.*, vol. 53, no. 2, pp. 453–471, Jan. 2008.

[13] C. Gabriel, A. Peyman, and E. H. Grant, "Electrical conductivity of tissue at frequencies below 1 MHz," *Phys. Med. Biol.*, vol. 54, no. 16, pp. 4863–4878, 2009.

[14] S. Gabriel, R. W. Lau, and C. Gabriel, "The dielectric properties of biological tissues: III. Parametric models for the dielectric spectrum of tissues," *Phys. Med. Biol.*, vol. 41, no. 11, pp. 2271–2293, Nov. 1996.

[15] R. Scorretti, N. Burais, O. Fabrègue, A. Nicolas, and L. Nicolas, "Computation of the induced current density into the human body due to relative LF magnetic field generated by realistic devices," *IEEE Trans. Mag.*, vol. 40, no. 2, pp. 643–646, 2004.

[16] A. Bossavit, *Computational Electromagnetism: Variational Formulations, Complementarity, Edge Elements*. San Diego, CA: Academic Press, 1998.

[17] R. Scorretti, R. Perrussel, L. Morel, N. Burais, and L. Nicolas, "Numerical dosimetry of currents induced in the human body by ELF magnetic fields," *COMPEL*, vol. 29, no. 6, pp. 1425–1434, 2010.

[18] Z. Ren, "Influence of the R.H.S. on the convergence behaviour of the curl-curl equation," *IEEE Trans. Mag.*, vol. 32, no. 3, pp. 655–658, 1996.

[19] C. Geuzaine, B. Meys, F. Henrotte, P. Dular, and W. Legros, "A Galerkin projection method for mixed finite elements," *IEEE Trans. Mag.*, vol. 35, no. 3, pp. 1438–1441, May 1999.

[20] J. Rikabi, C. Bryant, and E. Freeman, "An error-based approach to complementary formulations of static field solutions," *Int. J. Numer. Meth. Eng.*, vol. 26, no. 9, pp. 1963–1987, 1988.

[21] J. Penman, "Dual and complementary variational techniques for the calculation of electromagnetic fields," *Adv. Electron. Electron Phys.*, vol. 70, pp. 315–364, 1988.

[22] R. Albanese and R. Fresa, "Upper and lower bounds for local electromagnetic quantities," *Int. J. Numer. Meth. Eng.*, vol. 42, no. 3, pp. 499–515, 1998.

[23] A. Christ, W. Kainz, E. G. Hahn, K. Honegger, M. Zefferer, E. Neufeld, W. Rascher, R. Janka, W. Bautz, J. Chen, B. Kiefer, P. Schmitt, H.-P. Hollenbach, J. Shen, M. Oberle, D. Szczerba, A. Kam, J. W. Guag, and N. Kuster, "The virtual family-development of surface-based anatomical models of two adults and two children for dosimetric simulations," *Phys. Med. Biol.*, vol. 55, no. 2, pp. N23–N38, Jan. 2010.

[24] Q. Fang and D. Boas, "Tetrahedral mesh generation from volumetric binary and gray-scale images," in *Proc. IEEE Int. Symp. on Biomed. Imag.*, 2009, vol. Isbi, pp. 1142–1145.

[25] T. Dawson, K. Caputa, and M. Stuchly, "Electric fields induced in humans and rodents by 60 Hz magnetic fields," *Phys. Med. Biol.*, vol. 47, p. 2561, 2002.